IEEE Access
Multidisciplinary ⋮ Rapid Review ⋮ Open Access Journal

Received November 23, 2021, accepted December 15, 2021, date of publication December 16, 2021,
date of current version December 27, 2021.

Digital Object Identifier 10.1109/ACCESS.2021.3136242

Design and Control of a Reconfigurable Upper Limb Rehabilitation Exoskeleton With Soft Modular Joints

QUAN LIU[1], YANG LIU[1], CHANG ZHU[1], XINGXING GUO[1], WEI MENG[1,2], (Member, IEEE), QINGSONG AI[1], (Member, IEEE), AND JIWEI HU[1]

[1]School of Information Engineering, Wuhan University of Technology, Wuhan 430070, China
[2]Wuhan University of Technology Chongqing Research Institute, Chongqing 401135, China

Corresponding author: Jiwei Hu (hujiwei@whut.edu.cn)

This work was supported in part by the National Natural Science Foundation of China under Grant 52075404 and Grant 52075398, in part by the Research Project of the Chongqing Research Institute of Wuhan University of Technology under Grant YF2021-17, and in part by the Fundamental Research Funds for Central Universities under Grant WUT: 2021CG009.

ABSTRACT Upper limb rehabilitation robot can effectively help patients recover motor ability. Existing rehabilitation robots are usually driven by rigid motors and the mechanical structures cannot adapt to the different patients with the different physical parameters and different rehabilitation needs. This paper designs a reconfigurable upper limb rehabilitation exoskeleton for elbow and wrist joints driven by pneumatic muscle actuators (PMAs). The exoskeleton can assist patients to achieve elbow flexion/extension, wrist flexion/ extension and adduction/abduction by integrating soft elbow and wrist joint modules which can work separately or together. The wrist joint can realize two degrees of freedom (2-DoF) movement via adjustable modules. To conquer the dynamic model errors and load disturbances when reconstructing the modular joints, a non-singular fast terminal sliding mode control method based on nonlinear disturbance observer (NFTSMC-NDO) is proposed, and a position/force hierarchical control method is formed to ensure the controllability of the soft modular robot. Experimental results show that the proposed method can achieve high-precision motion control of soft modular joints and provide reconfigurable assistance for patients, improving the adaptability and compliance of rehabilitation training.

INDEX TERMS Upper limb rehabilitation, pneumatic muscles, reconfigurable exoskeleton, sliding mode control, nonlinear disturbance observer.

I. INTRODUCTION

Most stroke patients are accompanied by hemiplegia, which seriously affects patients' activities of daily living (ADL) [1]. Nearly 80% of stroke patients have upper limb dysfunction after surgery, but only 30% of them can eventually recover basic motor functions. Elbow and wrist joints are most frequently used in daily life and are the important carrier for people to engage in complex and fine motor function. The dysfunction of upper limb will have an adversely impact on patient's ADL. Traditional manual rehabilitation training is energy-consuming for both patients and physiotherapists, and rehabilitation evaluation is mostly subjective evaluation by the physiotherapists [2]. Rehabilitation robot is easy to operate which can effectively reduce the physical burden and the rehabilitation effect can be quantitatively evaluated through smart sensing. Some upper limb rehabilitation robots are based on end-effector [3], which could not provide accurate assisting torque for the joints of the upper limb. Rehabilitation exoskeleton is designed based on the bionic principle and comfortably wearable. The torque provided by exoskeleton is in coaxial with the joints of the upper limb, so the assistance torque can be accurately applied to the corresponding joint.

The structure of existing exoskeletons is usually fixed and the robot configuration will not change once manufactured. In comparison, reconfigurable modular design can facilitate the installation and disassembly of the exoskeleton, making the exoskeleton more flexible and adjustable to different patients with different physical parameters and different rehabilitation needs. Santos *et al.* [4] developed a modular lower limb rehabilitation exoskeleton composed of light tubular structure and six free joints. Garrido *et al.* [5] also designed a

The associate editor coordinating the review of this manuscript and approving it for publication was Vincenzo Conti.

This work is licensed under a Creative Commons Attribution 4.0 License. For more information, see https://creativecommons.org/licenses/by/4.0/

4-DOF upper limb exoskeleton with reconfigurable modular design. Reconfigurable design can be extended to more joints to increase the utilization rate and reduce the research costs.

Existing rehabilitation exoskeletons are mainly driven by rigid motors [6], [7], which is lack of compliance and easy to cause secondary injury. Ren *et al.* [8] developed a 10-DOF upper limb rehabilitation exoskeleton IntelliArm, including 8 active degrees of freedom and 2 passive degrees of freedom. The ETS-MARSE upper limb rehabilitation robot system driven by maxon motors is developed by Rahman *et al.* [9], which has 7 degrees of freedom. The rigid motor drivers can achieve high control accuracy but low compliance. In the case of excessive movement or sudden abnormal force, it is easy to cause secondary injury to the patient's affected limb. Compared with rigid motors, pneumatic muscle actuators (PMAs) have advantages of good safety, high compliance, light weight and low cost [10]. Tang *et al.* [11] developed a 1-DOF upper limb assistive device for elbow flexion/extension using PMAs. The wearable power-assisted exoskeleton RUPERT-IV developed by Zhang *et al.* [12] integrates soft actuators to collect real-time movement and posture data of the upper limb. Reconfigurable modular exoskeleton driven by PMAs can effectively improve the compliance and the adaptability for rehabilitation.

Reasonable mechanism design can ensure the safety and comfort of patients, and appropriate control algorithm can provide accurate trajectory tracking and seamless human-robot interaction [13], [14]. To address the nonlinear control challenges for exoskeleton, Zhu *et al.* [15] proposed a nonlinear iterative learning control algorithm by introducing nonlinear saturation functions to tackle the uncertainties in motion control. Fellag *et al.* [16] used sliding mode control to achieve accurate position control of a 5-DOF upper limb exoskeleton. The non-singular terminal sliding mode technique adopted by Madani *et al.* [17] can achieve convergence in finite time and avoid singularity. PMAs have strong coupling, nonlinearity, and time-varying characteristics, leading to difficult control. For rehabilitation robots driven by PMAs, Chang [18] adopted an adaptive self-organizing fuzzy sliding mode controller to the 2-DOF upper limb rehabilitation robots, which obtained good tracking performance. Zhang *et al.* [19] proposed an adaptive trajectory tracking control strategy with spatial force distribution, which contains position feedback in task space and force feedback in joint space to ensure the safety of soft robot control.

The dynamic complexity of reconfigurable exoskeleton is highly related to its mechanical structure and external interference. Reconfigurable modular design and the difference of patients with the different physical parameters will increase the uncertainty of dynamic model parameters. Wu *et al.* [20] proposed a fuzzy adaptive controller based on radial basis function on the 7-DOF upper limb rehabilitation exoskeleton to ensure the tracking accuracy under parameter uncertainty and environmental disturbance. The composite control strategy using disturbance observers combined with nonlinear methods can resist disturbance. For multi-input and multi-output systems with unknown external disturbances and uncertainties, Wu *et al.* [21] combined the interference observer and the TSM scheme to form a hybrid controller with strong anti-interference and anti-uncertainty capabilities. Wei and Zhang [22] combined the advantages of disturbance observers and backstepping method to tackle unknown disturbances and model uncertainties.

To address the problem of insufficient compliance and adaptability, this paper will combine soft actuators and reconfigurable modular design to provide patients with comfortable and safe rehabilitation training. Aiming at the load disturbance caused by the difference of patients with different physical parameters and the nonlinear characteristics of PMAs, a non-singular fast terminal sliding mode control method based on nonlinear disturbance observer (NFTSMC-NDO) is proposed. The improved control method can not only achieve accurate motion control, but also ensure to provide appropriate assistance torque to make the rehabilitation training more comfortable and effective. The main contributions of this work include: 1) A novel reconfigurable modular exoskeleton with the modules for elbow and wrist joints is designed and implemented for upper limb rehabilitation to enhance the adaptability and compliance of rehabilitation training. 2) To conquer the dynamic model errors and load disturbances when reconstructing the modular joints, and a non-singular terminal sliding mode control method based on nonlinear disturbance observer is proposed to reduce tracking error. 3) A force/ position hierarchical control method is proposed for the reconfigurable modular exoskeleton driven by PMAs based on NFTSMC-NDO to further improve the safety and compliance of human-robot inter action.

The rest of this paper is organized as follows. Section II describes the reconfigurable modular design of upper limb exoskeleton driven by PMAs, followed by the force/position hierarchical control method for the reconfigurable modular exoskeleton in Section III. Experimental results analysis of elbow and wrist joint modules is presented in Section IV, and the discussion and conclusion are drawn in Section V.

II. RECONFIGURABLE MODULAR DESIGN OF UPPER LIMB REHABILITATION EXOSKELETON

A. PMAs-DRIVEN SOFT MODULAR JOINTS

PMAs possess the characteristics of light weight and high compliance, but it can only generate pulling forces. To realize rotational motions, existing structures of antagonistic muscle pairs are shown in Figure 1. Compared with the other two structures, the pulley structure is easier to establish and can provide large joint torque, which is mostly adopted for the elbow and wrist modules of the upper limb exoskeleton.

The normal motion range of elbow (ROM) and wrist joints is shown in Table 1, as the reference standard for exoskeleton design. The zero-degree position of the elbow is defined that the upper arm droops naturally, and the forearm is 90 ° to the upper arm and parallel to the horizontal plane. The flexion

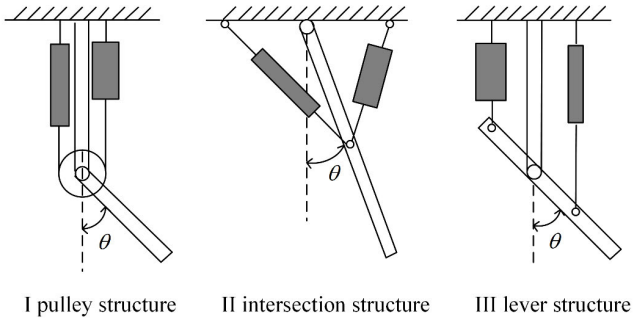

FIGURE 1. Modular joint structure with antagonistic PMAs.

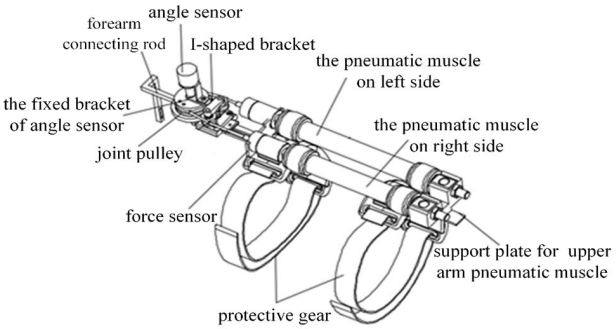

FIGURE 2. Mechanism design of the module for elbow joint.

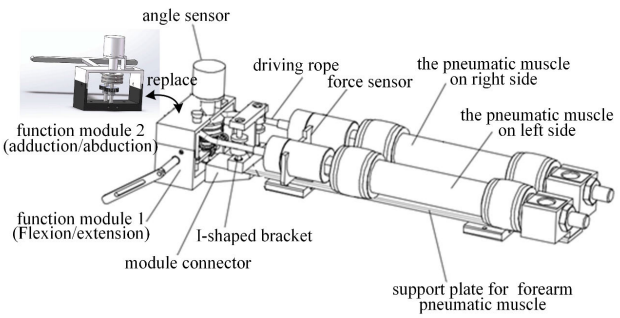

FIGURE 3. Mechanism design of the module for wrist joint.

of elbow joint is defined as negative and the extension of elbow joint is positive. Similarly, the zero-degree position of the wrist is defined that the palm faces down and the palm is in a straight line with the forearm. Then the flexion of wrist joint is defined as negative and the extension of wrist joint is positive, and the adduction of wrist joint is defined as negative and the abduction of wrist joint is defined as positive.

The modules for elbow and wrist joints are shown in Figure 2 and Figure 3, which mainly include the antagonistic PMAs, the support plate for PMAs, the joint pulley, the angle sensor and the force sensor. Modular designs enable personalized configuration to meet different rehabilitation requirements. When the forearm connecting rod is installed on the support plate of the modules for wrist joints, cooperative rehabilitation training of elbow and wrist joint can be realized,

TABLE 1. Range of Motion of Elbow and Wrist Joints.

Joints	Motions	Extreme ROM	Normal ROM
Elbow Joint	Flexion/Extension	-90°~50°	-90°~30°
Wrist Joint	Flexion/Extension	-30°~70°	-30°~50°
Wrist Joint	Adduction/Abduction	-35°~25°	-30°~20°

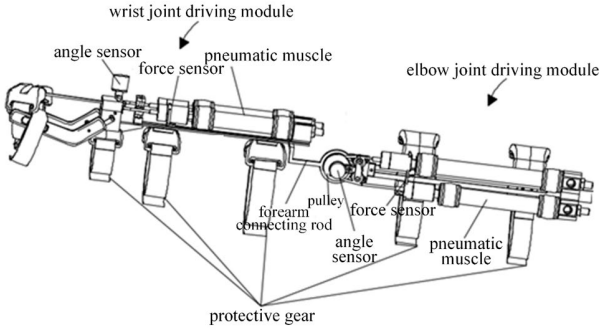

FIGURE 4. Reconfigurable modular design of the upper limb exoskeleton.

which mainly applies to the early-stage of rehabilitation. The protective gear can be separately installed on the upper arm or forearm connecting rod to fix the equipment, and the modules for elbow and wrist joints can be used independently for late-stage rehabilitation. During ADL training exercises, there is almost no inversion/eversion movement of the wrist joint, and the inversion and eversion of the palm occur in the radioulnar joint. Combined with the actual needs, only the most practical two degrees of freedom are designed for the wrist joint module of exoskeleton. The module for wrist joint has two degrees of freedom, of which module 1 is designed for flexion/extension, and module 2 for adduction/abduction. The conversion of the modules for wrist joint can change the degree of freedom.

B. RECONFIGURABLE MODULAR DESIGN

A reconfigurable upper limb rehabilitation exoskeleton with the soft modules for elbow and wrist joints is shown in Figure 4. The reconfigurable exoskeleton includes the modules for elbow and wrist joints, the module for joint connection, and the protective gear parts. The modules for elbow and wrist joints adopt antagonistic pneumatic muscle pairs combined with pulley structure to realize upper limb rehabilitation. The reconfigurable mechanism can improve utilization and compliance of the exoskeleton. The detachable and attachable design of the module for joint connection can not only realize compound training for patients with elbow-wrist dysfunction, but also provide separate training for elbow or wrist joint, and the conversion of wrist module can realize the mutual change from flexion/extension to adduction/adduction. According to patient's physical parameters, the 3D printed lightweight protective gear is customized to fit the upper limb and reduce the weight of the exoskeleton.

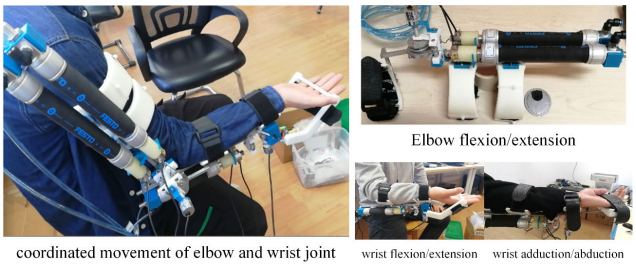

FIGURE 5. Implementation of the reconfigurable rehabilitation exoskeleton with the modules for elbow and wrist joints.

TABLE 2. Parameters of the adopted pneumatic muscles and pulleys.

Joints	Initial PMA length	Maximum shrinkage	Working pressure	Pulley radius
Elbow	16cm	25%	0~6bar	2cm
Wrist	9cm	25%	0~6bar	1cm

The installation of protective gear can be adjusted according to patient needs.

The designed reconfigurable exoskeleton adopts soft PMAs as the actuator to improve the compliance and safety of the device. The angle and force sensors can collect real-time motion data of patients and provide a hardware basis for the safe control of exoskeletons. The modules for elbow and wrist joints are connected in a detachable manner, which is convenient for disassembly and assembly, increasing the practicality and compliance of the device. The reconfigurable upper limb rehabilitation exoskeleton is shown in Figure 5, in which the customized 3D printed protective gear can fit the upper limb well, and the total weight of the exoskeleton is less than 2kg. The left figure shows the coordinated movement of elbow and wrist joint when the forearm connecting rod of the elbow joint is fixedly attached to the wrist module, and the right figures show the modules for elbow and wrist joints used separately. During control, the shoulder joint and elbow-wrist joint define an initial position, and the initial position is also shown in Figure 5. Each training starts at the initial position, and the shoulder posture has little effect on the actual control.

If the structural parameters of the exoskeleton cannot be adjusted, it only suits a small number of patients. To make the reconfigurable exoskeleton suitable for different patients with different physical parameters and different rehabilitation needs, the modules for elbow and wrist joints are designed adjustable: upper arm length: 250-350 mm (adjustable range: 100 mm), forearm length: 180-300 mm (adjustable range: 120 mm), wrist to handle (handle in the front of palm): 120-160 mm (adjustable range: 40 mm). Based on the above data, the parameters of the adopted PMAs and pulley are illustrated in Table 2.

To verify the reconfigurable modular exoskeleton's ability to help patients complete elbow flexion/extension, wrist flexion/ extension, and wrist adduction/abduction. The simulation experiment with the kinematic model is conducted to test the ROM of the reconfigurable upper limb exoskeleton.

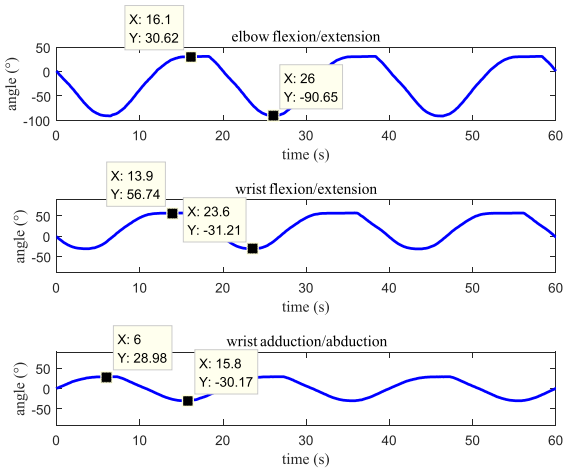

FIGURE 6. The ROM of the reconfigurable upper limb exoskeleton.

The ROM results are shown in Figure 6. Compare the normal ROM in Table 1, the ROM of the reconfigurable modular exoskeleton can meet the rehabilitation needs for elbow and wrist joints when the modules for elbow and wrist joints work separately. When the modules for elbow and wrist joints is reconstructed, i.e., both modules work together, the ROM of the elbow joint is slightly reduced due to the increased load of the elbow joint and the limit of the maximum input pressure of the PMAs. However, it still meets the most rehabilitation needs of elbow joint, and the ROM of the wrist joint remains unchanged.

III. POSITION/FORCE HIERARCHICAL CONTROL OF THE RECONFIGURABLE EXOSKELETON

A. THE DESIGN OF NONLINEAR DISTURBANCE OBSERVER

The premise of effective application of the upper limb rehabilitation exoskeleton is to realize its safe and stable motion control. On the one hand, the change of parameters such as center of gravity after exoskeleton wearing will lead to measurement error. On the other hand, different patients with various physical parameters and load disturbance will bring errors to the dynamics model. To tackle the control challenges for reconfigurable structure and the nonlinear disturbance during upper limb coordinated movement, a non-singular fast terminal sliding mode control method based on nonlinear disturbance observer (NFTSMC-NDO) is proposed to estimate and compensate the nonlinear disturbance.

Combined with the structural characteristics and training methods of upper limb exoskeleton, we only consider the dynamic modeling of the cooperative motion of elbow flexion / extension and wrist flexion / extension. To design a nonlinear disturbance observer, and the dynamic model established according to Figure 7 is:

$$\boldsymbol{M}(\boldsymbol{\theta})\ddot{\boldsymbol{\theta}} + \boldsymbol{C}\left(\boldsymbol{\theta}, \dot{\boldsymbol{\theta}}\right)\dot{\boldsymbol{\theta}} + \boldsymbol{G}(\boldsymbol{\theta}) = \boldsymbol{\tau} \tag{1}$$

$$\boldsymbol{\tau} = [\tau_1 \tau_2]^T ;\ \boldsymbol{\theta} = [\theta_1 \theta_2]^T ;\ \dot{\boldsymbol{\theta}} = \left[\dot{\theta}_1 \dot{\theta}_2\right]^T ;\ \ddot{\boldsymbol{\theta}} = \left[\ddot{\theta}_1 \ddot{\theta}_2\right]^T \tag{2}$$

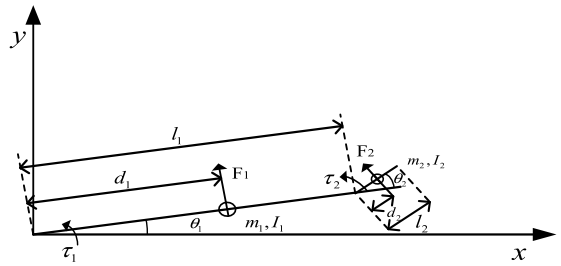

FIGURE 7. Dynamic model of elbow and wrist joint.

$$\boldsymbol{M}(\boldsymbol{\theta}) = \begin{bmatrix} m_1 d_1^2 + m_2\left(l_1^2 + d_2^2 + 2l_1 d_2 \cos\theta_2\right) + I_1 + I_2 & m_2\left(d_2^2 + l_1 d_2 \cos\theta_2\right) + I_2 \\ m_2\left(d_2^2 + l_1 d_2 \cos\theta_2\right) + I_2 & m_2 d_2^2 + I_2 \end{bmatrix} \tag{3}$$

$$\boldsymbol{C}\left(\boldsymbol{\theta}, \dot{\theta}\right) = \begin{bmatrix} -m_2 l_1 d_2 \dot{\theta}_2 \sin\theta_2 & -m_2 l_1 d_2 (\dot{\theta}_1 + \dot{\theta}_2) \sin\theta_2 \\ m_2 l_1 d_2 \dot{\theta}_1 \sin\theta_2 & 0 \end{bmatrix} \tag{4}$$

$$\boldsymbol{G}(\boldsymbol{\theta}) = \begin{bmatrix} (m_1 d_1 + m_2 l_1) g \cos\theta_1 + m_2 d_2 g \cos(\theta_1 + \theta_2) \\ m_2 d_2 g \cos(\theta_1 + \theta_2) \end{bmatrix} \tag{5}$$

where $\boldsymbol{\theta}, \dot{\boldsymbol{\theta}}, \ddot{\boldsymbol{\theta}} \in \boldsymbol{R}^n$ represents the joint angle, angular velocity and angular acceleration vector; $\boldsymbol{\tau} \in \boldsymbol{R}^n$ is joint torque; $\boldsymbol{M}(\boldsymbol{\theta})$ is the positive definite symmetric inertia matrix; $\boldsymbol{C}(\boldsymbol{\theta}, \dot{\boldsymbol{\theta}})$ is the centrifugal force and Coriolis force matrix; $\boldsymbol{G}(\boldsymbol{\theta})$ is the n-dimensional gravity item; m_1, m_2 is forearm and palm mass; l_1, l_2 is forearm and palm length; I_1, I_2 is moment of inertia; d_1, d_2 is distance from center of gravity to joint center.

Considering the disturbance factors, the system dynamics is:

$$[\boldsymbol{M}(\boldsymbol{\theta}) + \Delta\boldsymbol{M}(\boldsymbol{\theta})]\ddot{\boldsymbol{\theta}} + \left[\boldsymbol{C}\left(\boldsymbol{\theta}, \dot{\boldsymbol{\theta}}\right) + \Delta\boldsymbol{C}\left(\boldsymbol{\theta}, \dot{\boldsymbol{\theta}}\right)\right]\dot{\boldsymbol{\theta}} + [\boldsymbol{G}(\boldsymbol{\theta}) + \Delta\boldsymbol{G}(\boldsymbol{\theta})] = \boldsymbol{\tau} \tag{6}$$

$\boldsymbol{M}(\boldsymbol{\theta})$, $\boldsymbol{C}(\boldsymbol{\theta}, \dot{\boldsymbol{\theta}})$, $\boldsymbol{G}(\boldsymbol{\theta})$ is the nominal matrix of the model, and $\Delta\boldsymbol{M}(\boldsymbol{\theta})$, $\Delta\boldsymbol{C}(\boldsymbol{\theta}, \dot{\boldsymbol{\theta}})$, $\Delta\boldsymbol{G}(\boldsymbol{\theta})$ is the uncertain matrix of the model caused by load disturbance. Eq. (6) can be rewritten as:

$$\boldsymbol{M}(\boldsymbol{\theta})\ddot{\boldsymbol{\theta}} + \boldsymbol{C}(\boldsymbol{\theta}, \dot{\boldsymbol{\theta}})\dot{\boldsymbol{\theta}} + \boldsymbol{G}(\boldsymbol{\theta}) = \boldsymbol{\tau} + \boldsymbol{d} \tag{7}$$

where $\boldsymbol{d} = -\Delta\boldsymbol{M}(\boldsymbol{\theta})\ddot{\boldsymbol{\theta}} - \Delta\boldsymbol{C}(\boldsymbol{\theta}, \dot{\boldsymbol{\theta}})\dot{\boldsymbol{\theta}} - \Delta\boldsymbol{G}(\boldsymbol{\theta})$ is the load disturbance.

The nonlinear disturbance observer modifies the estimation result of the observer by the difference between the actual disturbance and the estimated disturbance.

Take $\dot{\tilde{\boldsymbol{d}}} = \boldsymbol{L}(\boldsymbol{\theta})(\boldsymbol{d} - \hat{\boldsymbol{d}})$ and define assistance parameter $z = \hat{d} - \boldsymbol{p}(\dot{\boldsymbol{\theta}})$, where $z \in \boldsymbol{R}^2$, and function vector $\boldsymbol{p}(\dot{\boldsymbol{\theta}})$ is:

Let

$$\dot{\boldsymbol{p}}(\dot{\boldsymbol{\theta}}) = \boldsymbol{L}(\boldsymbol{\theta})\boldsymbol{M}(\boldsymbol{\theta})\ddot{\boldsymbol{\theta}} \tag{8}$$

Then

$$\dot{z} = \dot{\hat{\boldsymbol{d}}} - \dot{\boldsymbol{p}}(\dot{\boldsymbol{\theta}}) = \dot{\hat{\boldsymbol{d}}} - \boldsymbol{L}(\boldsymbol{\theta})\boldsymbol{M}(\boldsymbol{\theta})\ddot{\boldsymbol{\theta}} \tag{9}$$

$$\dot{\hat{\boldsymbol{d}}} = \boldsymbol{L}(\boldsymbol{\theta})(\boldsymbol{M}(\boldsymbol{\theta})\ddot{\boldsymbol{\theta}} + \boldsymbol{C}(\boldsymbol{\theta}, \dot{\boldsymbol{\theta}})\dot{\boldsymbol{\theta}} + \boldsymbol{G}(\boldsymbol{\theta}) - \boldsymbol{\tau}) - \boldsymbol{L}(\boldsymbol{\theta})\hat{\boldsymbol{d}} \tag{10}$$

$$\dot{z} = \boldsymbol{L}(\boldsymbol{\theta})\left(\boldsymbol{C}\left(\boldsymbol{\theta}, \dot{\boldsymbol{\theta}}\right)\dot{\boldsymbol{\theta}} + \boldsymbol{G}(\boldsymbol{\theta}) - \boldsymbol{\tau}\right) - \boldsymbol{L}(\boldsymbol{\theta})\hat{\boldsymbol{d}} \tag{11}$$

The nonlinear disturbance observer is designed as:

$$\begin{cases} \dot{z} = \boldsymbol{L}(\boldsymbol{\theta})(\boldsymbol{C}(\boldsymbol{\theta}, \dot{\boldsymbol{\theta}})\dot{\boldsymbol{\theta}} + \boldsymbol{G}(\boldsymbol{\theta}) - \boldsymbol{\tau}) - \boldsymbol{L}(\boldsymbol{\theta})\hat{\boldsymbol{d}} \\ \hat{\boldsymbol{d}} = z + \boldsymbol{p}(\dot{\boldsymbol{\theta}}) \end{cases} \tag{12}$$

Then

$$\dot{z} = \boldsymbol{L}(\boldsymbol{\theta})\left(\boldsymbol{C}\left(\boldsymbol{\theta}, \dot{\boldsymbol{\theta}}\right)\dot{\boldsymbol{\theta}} + \boldsymbol{G}(\boldsymbol{\theta}) - \boldsymbol{\tau} - \boldsymbol{p}(\dot{\boldsymbol{\theta}})\right) - \boldsymbol{L}(\boldsymbol{\theta})z \tag{13}$$

Assume that the change of disturbance is slow compared to the dynamic characteristics of observer, that is $\dot{d} = 0$, then:

$$\dot{\tilde{\boldsymbol{d}}} = \dot{\boldsymbol{d}} - \dot{\hat{\boldsymbol{d}}} = -\dot{\hat{\boldsymbol{d}}} = -\dot{z} - \dot{\boldsymbol{p}}(\dot{\boldsymbol{\theta}}) \tag{14}$$

Substituting $\dot{\boldsymbol{p}}(\dot{\boldsymbol{\theta}}) = \boldsymbol{L}(\boldsymbol{\theta})\boldsymbol{M}(\boldsymbol{\theta})\ddot{\boldsymbol{\theta}}$ and $\dot{z}$ into Eq. (14):

$$\dot{\tilde{\boldsymbol{d}}} = \boldsymbol{L}(\boldsymbol{\theta})(z + \boldsymbol{p}(\dot{\boldsymbol{\theta}})) - \boldsymbol{L}(\boldsymbol{\theta})(\boldsymbol{M}(\boldsymbol{\theta})\ddot{\boldsymbol{\theta}} + \boldsymbol{C}(\boldsymbol{\theta}, \dot{\boldsymbol{\theta}})\dot{\boldsymbol{\theta}} + \boldsymbol{G}(\boldsymbol{\theta}) - \boldsymbol{\tau}) \tag{15}$$

Substituting Eq. (12) and Eq. (7) into the above equation:

$$\dot{\tilde{\boldsymbol{d}}} = \boldsymbol{L}(\boldsymbol{\theta})\hat{\boldsymbol{d}} - \boldsymbol{L}(\boldsymbol{\theta})\boldsymbol{d} = -\boldsymbol{L}(\boldsymbol{\theta})(\boldsymbol{d} - \hat{\boldsymbol{d}}) = -\boldsymbol{L}(\boldsymbol{\theta})\tilde{\boldsymbol{d}} \tag{16}$$

Therefore, the observation error equation is:

$$\dot{\tilde{\boldsymbol{d}}} + \boldsymbol{L}(\boldsymbol{\theta})\tilde{\boldsymbol{d}} = 0 \tag{17}$$

Design an appropriate gain matrix $\boldsymbol{M}(\boldsymbol{\theta})$, the estimated value $\hat{\boldsymbol{d}}$ can approach the disturbance $\boldsymbol{d}$ exponentially. The function vector $\boldsymbol{L}(\boldsymbol{\theta})$ and $\boldsymbol{p}(\dot{\boldsymbol{\theta}})$ in the observer Eq. (12) as:

$$\boldsymbol{L}(\boldsymbol{\theta}) = \boldsymbol{X}^{-1}\boldsymbol{M}^{-1}(\boldsymbol{\theta}) \tag{18}$$

$$\boldsymbol{p}(\dot{\boldsymbol{\theta}}) = \boldsymbol{X}^{-1}\dot{\boldsymbol{\theta}} \tag{19}$$

where $\boldsymbol{X}$ is an invertible matrix, which can be obtained by linear matrix inequality. Design the Lyapunov function as:

$$V_0 = \tilde{\boldsymbol{d}}^T \boldsymbol{X}^T \boldsymbol{M}(\boldsymbol{\theta})\boldsymbol{X}\tilde{\boldsymbol{d}} \tag{20}$$

where $(\boldsymbol{\theta}) = \boldsymbol{M}(\boldsymbol{\theta})^T > 0$.

From Eq. (17) and Eq. (18):

$$\dot{\tilde{\boldsymbol{d}}} = -\boldsymbol{L}(\boldsymbol{\theta})\tilde{\boldsymbol{d}} = -\boldsymbol{X}^{-1}\boldsymbol{M}^{-1}(\boldsymbol{\theta})\tilde{\boldsymbol{d}} \tag{21}$$

$$\dot{\tilde{\boldsymbol{d}}}^T = -\left(\boldsymbol{X}^{-1}\boldsymbol{M}^{-1}(\boldsymbol{\theta})\tilde{\boldsymbol{d}}\right)^T = -\tilde{\boldsymbol{d}}^T \boldsymbol{M}^{-T}(\boldsymbol{\theta})\boldsymbol{X}^{-T} \tag{22}$$

then

$$\begin{aligned} \dot{\boldsymbol{V}}_0 &= \dot{\tilde{\boldsymbol{d}}}^T \boldsymbol{X}^T \boldsymbol{M}(\boldsymbol{\theta})\boldsymbol{X}\tilde{\boldsymbol{d}} + \tilde{\boldsymbol{d}}^T \boldsymbol{X}^T \dot{\boldsymbol{M}}(\boldsymbol{\theta})\boldsymbol{X}\tilde{\boldsymbol{d}} + \tilde{\boldsymbol{d}}^T \boldsymbol{X}^T \boldsymbol{M}(\boldsymbol{\theta})\boldsymbol{X}\dot{\tilde{\boldsymbol{d}}} \\ &= -\tilde{\boldsymbol{d}}^T (\boldsymbol{X} - \boldsymbol{X}^T \dot{\boldsymbol{M}}(\boldsymbol{\theta})\boldsymbol{X} + \boldsymbol{X}^T)\tilde{\boldsymbol{d}} \end{aligned} \tag{23}$$

Construct inequality $\boldsymbol{X} + \boldsymbol{X}^T - \boldsymbol{X}^T \dot{\boldsymbol{M}}(\boldsymbol{\theta})\boldsymbol{X} \geq \boldsymbol{\Gamma}$, where $\boldsymbol{\Gamma} > 0$ is a positive definite symmetric matrix. Then there are $\dot{\boldsymbol{V}}_0 \leq -\tilde{\boldsymbol{d}}^T \boldsymbol{\Gamma}\tilde{\boldsymbol{d}} = -\boldsymbol{\Gamma}' V_0$, where $\boldsymbol{\Gamma}' > 0$. The larger the value of $\boldsymbol{\Gamma}$, the higher the accuracy and the faster the final convergence speed can realize, and the disturbance observer will converge exponentially. Let $\boldsymbol{Y} = \boldsymbol{X}^{-1}$, multiply $\boldsymbol{Y}^T = (\boldsymbol{X}^{-1})^T$ and $\boldsymbol{Y} = \boldsymbol{X}^{-1}$ by the left and right sides of the inequality to get:

$$\boldsymbol{Y}^T + \boldsymbol{Y} - \dot{\boldsymbol{M}}(\boldsymbol{\theta}) \geq \boldsymbol{Y}^T \boldsymbol{\Gamma}\boldsymbol{Y} \tag{24}$$

That is $\boldsymbol{Y}^T+\boldsymbol{Y}-\boldsymbol{Y}^T\boldsymbol{\Gamma}\boldsymbol{Y}\geq\dot{\boldsymbol{M}}(\boldsymbol{\theta})$, since $\left\|\dot{\boldsymbol{M}}(\boldsymbol{\theta})\right\|\leq\zeta$, then $\dot{\boldsymbol{M}}(\boldsymbol{\theta})\leq\zeta\boldsymbol{I}$, the sufficient condition for the above equation is $\boldsymbol{Y}^T+\boldsymbol{Y}-\boldsymbol{Y}^T\boldsymbol{\Gamma}\boldsymbol{Y}\geq\zeta\boldsymbol{I}$, namely $\boldsymbol{Y}^T+\boldsymbol{Y}-\zeta\boldsymbol{I}-\boldsymbol{Y}^T\boldsymbol{\Gamma}\boldsymbol{Y}\geq 0$.

According to Schur's complement theorem: $\boldsymbol{C}$ is a positive definite matrix, and $\boldsymbol{A}-\boldsymbol{B}\boldsymbol{C}^{-1}\boldsymbol{B}^T\geq 0$ is equivalent to $\begin{bmatrix}\boldsymbol{A}\ \boldsymbol{B}\\ \boldsymbol{B}^T\ \boldsymbol{C}\end{bmatrix}\geq 0$. Finally, the above equation is equivalent to $\begin{bmatrix}\boldsymbol{Y}^T+\boldsymbol{Y}-\zeta\boldsymbol{I}\ \boldsymbol{Y}^T\\ \boldsymbol{Y}\ \boldsymbol{\Gamma}^{-1}\end{bmatrix}\geq 0$.

B. NON-SINGULAR FAST TERMINAL SLIDING MODE CONTROL

Terminal sliding mode control methods introduce nonlinear functions into the sliding mode surfaces. To solve the singularity problem, the sliding mode surface needs to be further improved. A non-singular terminal sliding mode control method was proposed in [23], where a non-singular fast terminal sliding mode surface is designed to improve the convergence:

$$\boldsymbol{s}=\boldsymbol{e}+\boldsymbol{H}sig(\boldsymbol{e})^{\boldsymbol{\alpha}}+\boldsymbol{K}sig(\dot{\boldsymbol{e}})^{\boldsymbol{\beta}} \tag{25}$$

$\boldsymbol{s}=[s_1,s_2,\cdots,s_n]^T\in\boldsymbol{R}^n$; $\boldsymbol{e}(t)$ is the angle tracking error, i.e., $\boldsymbol{e}(t)=\boldsymbol{\theta}(t)-\boldsymbol{\theta}_d(t)$; matrix $\boldsymbol{H}=diag(h_1,h_2,\cdots,h_n)$, $\boldsymbol{K}=diag(k_1,k_2,\cdots,k_n)$, $h_1,h_2,\cdots,h_n,k_1,k_2,\cdots,k_n$ is constant >0, $\boldsymbol{\alpha}=diag(\alpha_1,\alpha_2,\cdots,\alpha_n)$, $\boldsymbol{\beta}=diag(\beta_1,\beta_2,\cdots,\beta_n)$, $1<\beta_i<2,\alpha_i>\beta_i$; $sig(\boldsymbol{e})^{\boldsymbol{\alpha}}=\left[|e_1|^{\alpha_1}sgn(e_1),\cdots,|e_n|^{\alpha_n}sgn(e_n)\right]^T$, and the representation of $sig(\dot{\boldsymbol{e}})^{\boldsymbol{\beta}}$ is similar to that of $sig(\boldsymbol{e})^{\boldsymbol{\alpha}}$.

According to the designed sliding mode surface and the dynamic models of the system, a non-singular fast terminal sliding mode control method based on nonlinear disturbance observer is proposed to estimate and compensate the nonlinear disturbance. Combined with non-singular fast terminal sliding mode control (NFTSMC) and the disturbance observer, the final control law can be obtained as:

$$\begin{cases}\boldsymbol{\tau}=\boldsymbol{M}(\boldsymbol{\theta})\ddot{\boldsymbol{\theta}}_d+\boldsymbol{C}\left(\boldsymbol{\theta},\dot{\boldsymbol{\theta}}\right)\dot{\boldsymbol{\theta}}+\boldsymbol{G}(\boldsymbol{\theta})-\hat{\boldsymbol{d}}\\ -\boldsymbol{M}\boldsymbol{K}^{-1}\boldsymbol{\beta}^{-1}(\boldsymbol{I}_n+\boldsymbol{H}\boldsymbol{\alpha}diag(|e_i|^{\alpha_i-1}))sig(\dot{\boldsymbol{e}})^{2\boldsymbol{I}_n-\boldsymbol{\beta}}\\ \quad-\boldsymbol{M}\left[\boldsymbol{Y}_1\boldsymbol{s}+\boldsymbol{Y}_2sig(\boldsymbol{s})^{\boldsymbol{\gamma}}\right]\\ \begin{cases}\dot{\boldsymbol{z}}=\boldsymbol{L}(\boldsymbol{\theta})\left(\boldsymbol{C}\left(\boldsymbol{\theta},\dot{\boldsymbol{\theta}}\right)\dot{\boldsymbol{\theta}}+\boldsymbol{G}(\boldsymbol{\theta})-\boldsymbol{\tau}\right)-\boldsymbol{L}(\boldsymbol{\theta})\hat{\boldsymbol{d}}\\ \hat{\boldsymbol{d}}=\boldsymbol{z}+\boldsymbol{p}\left(\dot{\boldsymbol{\theta}}\right)\end{cases}\\ \boldsymbol{L}(\boldsymbol{\theta})=\boldsymbol{X}^{-1}\boldsymbol{M}^{-1}(\boldsymbol{\theta})\\ \boldsymbol{p}\left(\dot{\boldsymbol{\theta}}\right)=\boldsymbol{X}^{-1}\dot{\boldsymbol{\theta}}\end{cases} \tag{26}$$

where $\boldsymbol{I}_n$ is the identity matrix; $\boldsymbol{Y}_1=diag(y_{11},\cdots,y_{1n})$, $\boldsymbol{Y}_2=diag(y_{21},\cdots,y_{2n})$, y_{1i},y_{2i} are constants greater than 0; $\boldsymbol{\gamma}=diag(\gamma_1,\gamma_2,\cdots,\gamma_n)$, $0<\gamma_1,\gamma_2,\cdots,\gamma_n<1$. The robot joint output torque $\boldsymbol{\tau}$ includes the disturbance estimator $\hat{\boldsymbol{d}}$, the value of which observed by the designed disturbance observer.

The stability of the proposed NFTSMC needs to be analysed, and the Lyapunov function is designed as:

$$V=\frac{1}{2}\boldsymbol{s}^T\boldsymbol{s}+\tilde{\boldsymbol{d}}^T\boldsymbol{X}^T\boldsymbol{M}(\boldsymbol{\theta})\boldsymbol{X}\tilde{\boldsymbol{d}} \tag{27}$$

$$\dot{\boldsymbol{V}}=\boldsymbol{s}^T\dot{\boldsymbol{s}}-\tilde{\boldsymbol{d}}^T\left(\boldsymbol{X}-\boldsymbol{X}^T\dot{\boldsymbol{M}}(\boldsymbol{\theta})\boldsymbol{X}+\boldsymbol{X}^T\right)\tilde{\boldsymbol{d}} \tag{28}$$

Substituting Eq. (26) into Eq. (28) gives:

$$\begin{aligned}\dot{\boldsymbol{V}}=&\boldsymbol{s}^T\boldsymbol{K}\boldsymbol{\beta}diag(|\dot{\boldsymbol{e}}_i|^{\beta_i-1})\left[-\left(\boldsymbol{Y}_1\boldsymbol{s}+\boldsymbol{Y}_2sig(\boldsymbol{s})^{\boldsymbol{\gamma}}\right)\right.\\&\left.-\boldsymbol{M}^{-1}\left(\hat{\boldsymbol{d}}-\boldsymbol{d}\right)\right]-\tilde{\boldsymbol{d}}^T\left(\boldsymbol{X}-\boldsymbol{X}^T\dot{\boldsymbol{M}}(\boldsymbol{\theta})\boldsymbol{X}+\boldsymbol{X}^T\right)\tilde{\boldsymbol{d}}\\ \dot{\boldsymbol{V}}=&-\boldsymbol{s}^T\boldsymbol{K}\boldsymbol{\beta}diag(|\dot{\boldsymbol{e}}_i|^{\beta_i-1})\boldsymbol{Y}_1\boldsymbol{s}-\boldsymbol{s}^T\boldsymbol{K}\boldsymbol{\beta}diag(|\dot{\boldsymbol{e}}_i|^{\beta_i-1})\\&\boldsymbol{Y}_2sig(\boldsymbol{s})^{\boldsymbol{\gamma}}+\boldsymbol{s}^T\boldsymbol{K}\boldsymbol{\beta}diag(|\dot{\boldsymbol{e}}_i|^{\beta_i-1})\boldsymbol{M}^{-1}\tilde{\boldsymbol{d}}\\&-\tilde{\boldsymbol{d}}^T(\boldsymbol{X}-\boldsymbol{X}^T\dot{\boldsymbol{M}}(\boldsymbol{\theta})\boldsymbol{X}+\boldsymbol{X}^T)\tilde{\boldsymbol{d}}\end{aligned} \tag{29}$$

Finally,

$$\begin{aligned}\dot{\boldsymbol{V}}\leq&-2\underline{y}_1\boldsymbol{V}-2^{(\gamma+1)/2}\underline{y}_2\boldsymbol{V}^{(\gamma+1)/2}\\&+\boldsymbol{s}^T\boldsymbol{K}\boldsymbol{\beta}diag(|\dot{\boldsymbol{e}}_i|^{\beta_i-1})\boldsymbol{M}^{-1}\tilde{\boldsymbol{d}}-\tilde{\boldsymbol{d}}^T(\boldsymbol{X}-\boldsymbol{X}^T\dot{\boldsymbol{M}}(\boldsymbol{\theta})\boldsymbol{X}\\&+\boldsymbol{X}^T)\tilde{\boldsymbol{d}}\end{aligned} \tag{30}$$

Thus, $\dot{\boldsymbol{V}}_0=-\tilde{\boldsymbol{d}}^T(\boldsymbol{X}-\boldsymbol{X}^T\dot{\boldsymbol{M}}(\boldsymbol{\theta})\boldsymbol{X}+\boldsymbol{X}^T)\tilde{\boldsymbol{d}}$. The disturbance observer converges exponentially and the error converges to zero. $V_0=0,\tilde{\boldsymbol{d}}=0$, $\dot{\boldsymbol{V}}\leq-\boldsymbol{s}^T\boldsymbol{K}\boldsymbol{\beta}diag(|\dot{\boldsymbol{e}}_i|^{\beta_i-1})\left[(\boldsymbol{Y}_1\boldsymbol{s}+\boldsymbol{Y}_2sig(\boldsymbol{s})^{\boldsymbol{\gamma}})\right]$, then $\dot{\boldsymbol{V}}\leq-2\underline{y}_1\boldsymbol{V}-2^{(\gamma+1)/2}\underline{y}_2\boldsymbol{V}^{(\gamma+1)/2}$. The sliding mode surface of the system can reach $\boldsymbol{s}=\boldsymbol{0}$ in a finite time, and the trajectory tracking error converges to zero in a finite time along the sliding mode surface.

C. FORCE CONTROL OF SOFT MODULAR JOINTS

PMAs can only generate tension force rather than thrust, and antagonistic PMAs adopt the pulley structure. The relationship between the joint output torque of exoskeleton and the output force of antagonistic PMAs is as follows:

$$\tau=(F_2-F_1)\cdot r \tag{31}$$

where r is the radius of the pulley.

Once the joint output torque is given, the output force difference between the antagonistic PMAs is fixed, but there are multiple solutions for the specific value.

The force distribution method adopted for the antagonistic PMAs is as follows:

$$\begin{aligned}F_1&=\begin{cases}F_0 & if\ \tau\geq 0\\ \dfrac{|\tau|}{r}+F_0 & if\ \tau<0\end{cases}\\ F_2&=\begin{cases}\dfrac{|\tau|}{r}+F_0 & if\ \tau\geq 0\\ F_0 & if\ \tau<0\end{cases}\end{aligned} \tag{32}$$

As the characteristics of the PMAs are similar to Bowden cables, which can only provide tension force. If the minimum output force F_0 become negative, the driving ropes of the PMAs will be in a relaxed state [13], and the pulley structure may be out of control. In order to ensure that the driving ropes of the PMAs always maintains the stretched state, the appropriate solution F_1,F_2 for the output force of each PMA is obtained by setting the minimum output force $F_0=5N$, which needs to be greater than zero.

In order to achieve precise trajectory control, while ensuring that the driving ropes of the PMAs maintains a stretched

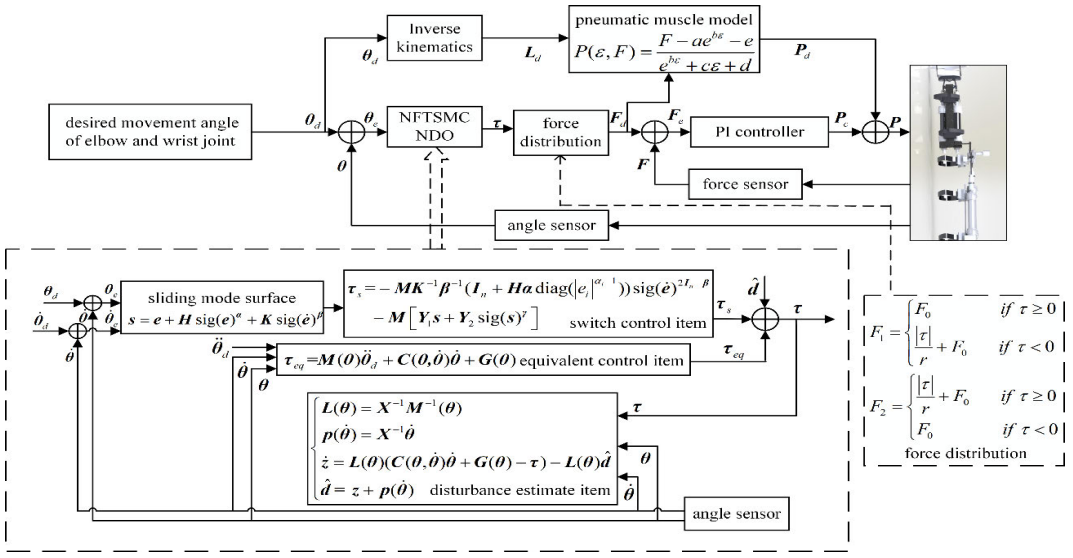

FIGURE 8. Diagram of the exoskeleton control system with non-singular fast terminal sliding mode control.

state to provide appropriate assistance torque during rehabilitation, a force/position hierarchical controller based on NFTSMC-NDO is proposed to realize the position and force control of the exoskeleton. The complete force/position hierarchical control block diagram is shown in Figure 7. The outer loop is position control, and the inner loop is force control. Based on the established dynamic model, the NFTSMC-NDO method is used to obtain the expected output torque of the exoskeleton, and the expected force of each PMA is obtained through force distribution method. Finally, through the static contraction model of the PMAs, the input air pressure is determined by the contraction displacement and the output force.

The exoskeleton reaches the final air pressure by using the desired air pressure and the adjusted output of the air pressure, so as to realize the control of the antagonistic PMAs. Firstly, the desired trajectory (x, y) of the exoskeleton is solved by inverse kinematics to obtain the corresponding expected joint angles $(\theta_{d1}, \theta_{d2})$. The expected joint angles $(\theta_{d1}, \theta_{d2})$ and the actual joint angles (θ_1, θ_2) collected by the angle sensors are used as input to the non-singular fast terminal sliding mode controller. Next, the expected output torque (τ_1, τ_2) corresponding to the joint is obtained through the controller, and the expected output force of each PMA $F_{11}, F_{12}, F_{21}, F_{22}$ is obtained through the force distribution method. Then, the expected joint angles $(\theta_{d1}, \theta_{d2})$ can be converted to the expected displacement $L_{d11}, L_{d12}, L_{d21}, L_{d22}$ of each PMA, and the expected contraction rate L_d/L_{ini} and output force F of the PMAs are substituted into the static contraction model of the PMAs to obtain the desired air pressure $P_{d11}, P_{d12}, P_{d21}, P_{d22}$. Finally, the difference between the expected output force of the PMA and the actual output force measured by the force sensor is used as the input to the proportional integral (PI) controller, and the adjusted output

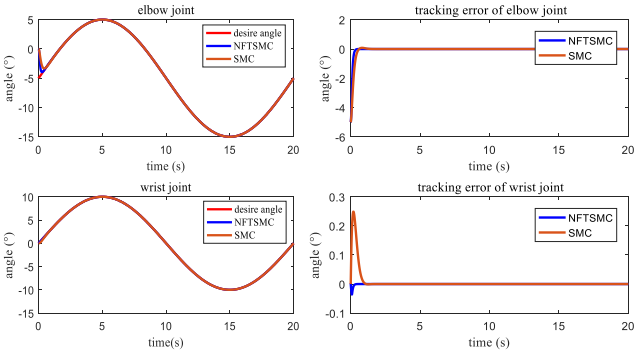

FIGURE 9. Angle tracking results using basic sliding mode control (SMC) and non-singular fast terminal sliding mode control (NFTSMC).

$P_{c11}, P_{c12}, P_{c21}, P_{c22}$ of the air pressure is obtained. The letter subscripts 11, 12, 21 and 22 respectively represent the PMA on the left side of elbow joint, the PMA on the right side of elbow joint, the PMA on the left side of wrist joint, and the PMA on the right side of wrist joint.

IV. EXPERIMENT RESULTS AND DISCUSSION

To verify the feasibility and effectiveness of the designed exoskeleton and the proposed control strategy, the simulation analysis was firstly performed in Simulink. The dynamic model shown in Figure 7 is adopted, and the specific parameter settings are as follows: $l_1 = 0.25m$, $m_1 = 1.625kg$, $d_1 = @zero.125m$, $l_2 = 0.12m$, $m_2 = 0.452kg$, $d_2 = 0.08m$. The desired angles of the elbow and wrist joint are: $\theta_1 = 10 * sin(0.1 * pi * t) - 5$ and $\theta_2 = 10 * sin(0.1 * pi * t)$, and the unit is angle (°). The simulation duration is set to 20s.

Experiment (1): When there is no disturbance in the system, the angle tracking results of basic sliding mode control (SMC) and non-singular fast terminal sliding mode

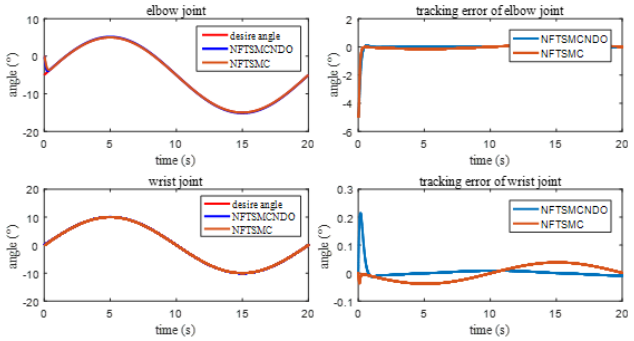

FIGURE 10. Angle tracking results using NFTSMC and non-singular fast terminal sliding mode based on nonlinear disturbance observer (NFTSMCNDO).

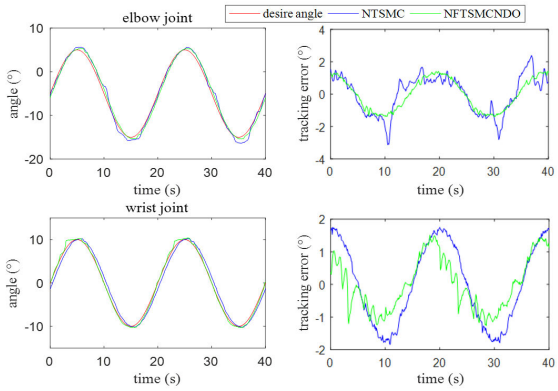

FIGURE 11. Angle tracking results of elbow and wrist joints with a participant using NTSMC and NFTSMCNDO.

control (NFTSMC) is compared, and the angle tracking results of the two methods under the same expected trajectory are shown in Figure 9. Both methods can achieve low tracking errors of the elbow and wrist joint with no disturbance, which verifies the feasibility of the control method. The response time of SMC before reaching stable state is 1.288s for the elbow joint and 1.044s for the wrist joint, while the response time of NFTSMC is 0.492s for the elbow joint and 0.3397s for the wrist joint, which shows that NFTSMC can respond quickly to the expected trajectory.

Experiment (2): When there is system disturbance, the angle tracking results of NFTSMC and NFTSMCNDO are compared, and the angle tracking results of the two methods under the same disturbance are shown in Figure 10. To verify the control effects using a nonlinear disturbance observer, the disturbance is set to $\mathrm{d} = \begin{bmatrix} 0.2 * sin(0.1 * pi * t) \\ 0.05 * sin(0.1 * pi * t) \end{bmatrix} (N \cdot m)$. It can be seen from Figure 9 and 10 that the tracking error of NFTSMC increases under disturbance. With the same initial state and disturbance, the average error of the elbow and wrist joint using NFTSMC are 0.1288° and 0.0245°, respectively. In comparison, the average error of the elbow and wrist joint of NFTSMCNDO are 0.0607° and 0.0088°, respectively, which is significantly reduced compared to NFTSMC. The simulation analysis verifies that NFTSMCNDO can ensure low tracking errors and faster convergence under disturbance for the exoskeleton.

In practical applications, the control accuracy might also be affected by various environmental factors (such as the sensor accuracy or system noises). The NTSMC method [17] and the NFTSMCNDO method proposed in this paper are used to realize the force/position hierarchical controller. A participant subject with a height of 176cm and a weight of 64kg was recruited to wear the upper limb exoskeleton for robot-assisted training, and the subject keeps the forearm and wrist in a relaxed state during the test. The desired angles of the elbow joint and the wrist joint are: $\theta_1 = 10 * sin(0.1 * pi * t) - 5$, $\theta_2 = 10 * sin(0.1 * pi * t)$, and the unit is angle (°). The experimental results are shown in Figure 11.

Table 3 shows that the tracking errors of the elbow and wrist joints reveals that the force/position hierarchical

TABLE 3. Statistics of tracking errors using two Control Methods.

Control Methods	Elbow Joint		Wrist Joint	
	ME (°)	AE (°)	ME (°)	AE (°)
NTSMC	3.1301	1.0272	1.8401	1.0857
NFTSMCNDO	1.4191	0.8724	1.5152	0.6945

controller based on NFTSMCNDO has better performance than NTSMC. The maximum error (ME) and the average error (AE) of the angle tracking result are used as indicators to compare the control performance. Taking the elbow joint as an example, the ME and AE of NTSMC is 3.1301° and 1.0272°, respectively, while the ME and AE of NFTSMCNDO is 1.4191° and 0.8724°, respectively. The maximum angle tracking error of the wrist joint using NTSMC is 1.8401° at around 20s, and the maximum angle tracking error of the elbow joint using NFTSMCNDO of 1.5152° at around 20s. In contrast, the ME and AE decreased by 54.7% and 15.07%, respectively. When the subject wears the upper limb exoskeleton under disturbances, the proposed NFTSMCNDO method can achieve low tracking errors, and the AE during the entire rehabilitation is small.

The NFTSMCNDO-based hierarchical controller uses PI controller at the inner loop, driving the PMAs in contracted state to track the desired output force. Figures 12 and 13 are the joint torque and output force of PMA tracking results of the force/position hierarchical controller with NFTSMCNDO in position loop and PI controller in force loop, respectively.

The results shown in Figure 12 indicate that the assistance torque of the elbow joint can basically meet the tracking effect, and the maximum tracking error is 0.65N·m. The tracking effect of the wrist joint torque is poor, and the maximum tracking error is 0.0635N·m. However, the desired wrist joint torque is small, and the actual torque is basically in line with the change trend of the desired torque. The output force of PMA tracking results is shown in Figure 13, and the error of force tracking control is larger than that of angle tracking control, Taking the elbow joint as an example, the ME and

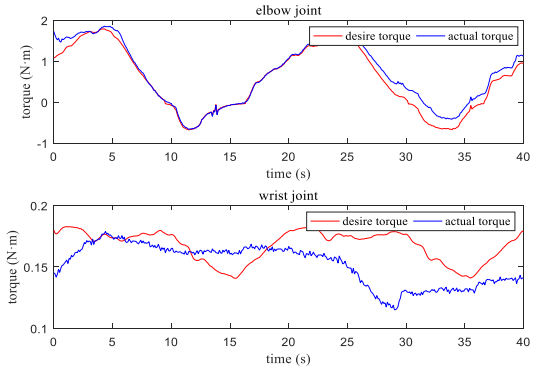

FIGURE 12. Joint torque tracking results of elbow and wrist joints.

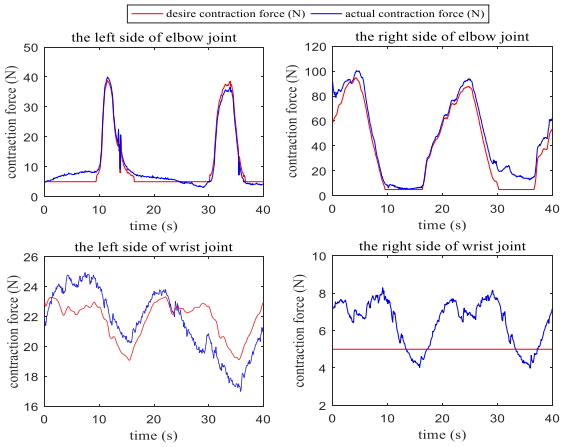

FIGURE 13. PMA output force results in elbow and wrist joints.

AE of the force tracking at the left PMA is 3.6374N and 1.5049N, respectively. The ME and AE of the force tracking at the right PMA is 32.3535N and 6.6754N, respectively. The goal of the position/force hierarchical controller is to ensure that the exoskeleton meets the angle control accuracy while the driving ropes of the PMAs maintains a stretched state. Though the force tracking accuracy is reduced, the actual contraction force is basically in the state of $F \geq 5N$ during the entire rehabilitation, which verifies the feasibility and effectiveness of position/force hierarchical controller.

According to the above comprehensive analysis, it can be concluded that the proposed force/position hierarchical control based on NFTSMCNDO can achieve high-precision angle control and better tracking performance. In addition, the contraction force of the PMAs in joint space are effectively controlled to ensure that all the driving ropes of the PMAs is kept in tension, and the operation safety of robot during rehabilitation is guaranteed. The configuration of traditional upper limb rehabilitation robot is often fixed. Due to the upper limb rehabilitation exoskeleton with reconfigurable modular mechanism and soft actuators, the uncertainties of the dynamic model will affect the high-precision control. The nonlinear disturbance observer can estimate and compensate the nonlinear disturbance of the system to effectively improve the control accuracy. Current rehabilitation robots driven by soft actuators basically do not consider force control in improving the stability of position control and safety in rehabilitation training. However, the position/force hierarchical control based on NFTSMCNDO can effectively ensure the control stability and safety of the exoskeleton.

V. CONCLUSION

In this paper, we designed a reconfigurable upper limb rehabilitation exoskeleton driven by soft actuators to help patients carry out safe and efficient rehabilitation training. Compared with the mechanism driven by rigid motors, the designed rehabilitation exoskeleton driven by the PMAs has the characteristics of light weight, small space occupation and high compliance. The reconfigurable modular mechanism is adopted in which the modules for elbow and wrist joints can be flexibly reconstructed to meet different rehabilitation needs of different patients with different physical parameters, and reconfigurable modular design has potential to increase the equipment utilization rate and reduce the research cost. Considering the load disturbance after reconstruction, the nonlinear disturbance observer is used to estimate and compensate the disturbance, and a position/force control method based on NFTSMCNDO is formed. The experimental results show that the position/force hierarchical controller can not only achieve precise position control, but also provide appropriate assistance torque, thereby making the rehabilitation training compliant and effective.

REFERENCES

[1] L. D. Wang, J. M. Liu, and Y. Yang, "The prevention and treatment of stroke still face huge challenges—Brief report on stroke prevention and treatment in China," *Chin. Circulat. J.*, vol. 34, no. 2, pp. 6–20, 2019.

[2] Z. G. Hou, X. G. Zhao, and L. Cheng, "Recent advances in rehabilitation robots and intelligent assistance systems," *Acta Autom. Sinica*, vol. 42, no. 12, pp. 1765–1779, 2016.

[3] S. K. Charles, H. I. Krebs, B. T. Volpe, D. Lynch, and N. Hogan, "Wrist rehabilitation following stroke: Initial clinical results," in *Proc. 9th Int. Conf. Rehabil. Robot.*, Jun. 2005, pp. 13–16.

[4] W. M. dos Santos, S. L. Nogueira, G. C. de Oliveira, G. G. Pena, and A. A. G. Siqueira, "Design and evaluation of a modular lower limb exoskeleton for rehabilitation," in *Proc. Int. Conf. Rehabil. Robot. (ICORR)*, Jul. 2017, pp. 447–451.

[5] J. Garrido, W. Yu, and X. Li, "Modular design and control of an upper limb exoskeleton," *J. Mech. Sci. Technol.*, vol. 30, no. 5, pp. 2265–2271, May 2016.

[6] J. M. Xue, "Development of medical exoskeleton rehabilitation robot," *Med. Inf.*, vol. 32, no. 9, pp. 19–21, 2019.

[7] T. Nef, M. Mihelj, and R. Riener, "ARMin: A robot for patient-cooperative arm therapy," *Med. Biol. Eng. Comput.*, vol. 45, pp. 887–900, Sep. 2007.

[8] Y. Ren, H.-S. Park, and L.-Q. Zhang, "Developing a whole-arm exoskeleton robot with hand opening and closing mechanism for upper limb stroke rehabilitation," in *Proc. IEEE Int. Conf. Rehabil. Robot.*, Jun. 2009, pp. 761–765.

[9] M. H. Rahman, T. K. Ouimet, M. Saad, J. P. Kenne, and P. S. Archambault, "Development and control of a wearable robot for rehabilitation of elbow and shoulder joint movements," in *Proc. 36th Annu. Conf. IEEE Ind. Electron. Soc. (IECON)*, Nov. 2010, pp. 1500–1505.

[10] T. Teramae, K. Ishihara, J. Babič, J. Morimoto, and E. Oztop, "Human-in-the-loop control and task learning for pneumatically actuated muscle based robots," *Frontiers Neurorobotics*, vol. 12, pp. 1–10, Nov. 2018.

[11] Z. Tang, K. Zhang, S. Sun, Z. Gao, L. Zhang, and Z. Yang, "An upper-limb power-assist exoskeleton using proportional myoelectric control," *Sensors*, vol. 14, no. 4, pp. 6677–6694, 2014.

[12] H. Zhang, H. Austin, S. Buchanan, R. Herman, J. Koeneman, and J. He, "Feasibility study of robot-assisted stroke rehabilitation at home using RUPERT," in *Proc. IEEE/ICME Int. Conf. Complex Med. Eng.*, May 2011, pp. 604–609.
[13] B. Ugurlu, P. Forni, C. Doppmann, E. Sariyildiz, and J. Morimoto, "Stable control of force, position, and stiffness for robot joints powered via pneumatic muscles," *IEEE Trans. Ind. Informat.*, vol. 15, no. 12, pp. 6270–6279, Dec. 2019.
[14] M. Hamaya, T. Matsubara, T. Teramae, T. Noda, and J. Morimoto, "Design of physical user–robot interactions for model identification of soft actuators on exoskeleton robots," *Int. J. Robot. Res.*, vol. 40, no. 1, pp. 397–410, Jan. 2021.
[15] X. Zhu, J. Wang, and X. Wang, "Nonlinear iterative learning control of 5 DOF upper-limb rehabilitation robot," in *Proc. IEEE Int. Conf. Robot. Biomimetics (ROBIO)*, Dec. 2015, pp. 793–798.
[16] R. Fellag, T. Benyahia, M. Drias, M. Guiatni, and M. Hamerlain, "Sliding mode control of a 5 DoFs upper limb exoskeleton robot," in *Proc. 5th Int. Conf. Electr. Eng.-Boumerdes (ICEE-B)*, Oct. 2017, pp. 57–62.
[17] T. Madani, B. Daachi, and K. Djouani, "Non-singular terminal sliding mode controller: Application to an actuated exoskeleton," *Mechatronics*, vol. 33, pp. 136–145, Feb. 2016.
[18] M.-K. Chang, "An adaptive self-organizing fuzzy sliding mode controller for a 2-DOF rehabilitation robot actuated by pneumatic muscle actuators," *Control Eng. Pract.*, vol. 18, no. 1, pp. 13–22, 2010.
[19] M. Zhang, A. McDaid, A. J. Veale, Y. Peng, and S. Q. Xie, "Adaptive trajectory tracking control of a parallel ankle rehabilitation robot with joint-space force distribution," *IEEE Access*, vol. 7, pp. 85812–85820, 2019.
[20] Q. Wu, X. Wang, B. Chen, and H. Wu, "Development of an RBFN-based neural-fuzzy adaptive control strategy for an upper limb rehabilitation exoskeleton," *Mechatronics*, vol. 53, pp. 85–94, Aug. 2018.
[21] Y.-J. Wu, J.-X. Zuo, and L.-H. Sun, "Adaptive terminal sliding mode control for hypersonic flight vehicles with strictly lower convex function based nonlinear disturbance observer," *ISA Trans.*, vol. 71, no. 2, pp. 215–226, Nov. 2017.
[22] X. J. Wei and L. Y. Zhang, "Anti-disturbance control based on disturbance observer for a class of nonlinear strict-feedback systems," *Control Decis.*, vol. 31, no. 9, pp. 1697–1701, 2016.
[23] P. Yang, X. Ma, J. Wang, G. Zhang, Y. Zhang, and L. Chen, "Disturbance observer-based terminal sliding mode control of a 5-DOF upper-limb exoskeleton robot," *IEEE Access*, vol. 7, pp. 62833–62839, 2019.

QUAN LIU received the Ph.D. degree in mechanical engineering from the Wuhan University of Technology, Wuhan, China, in 2003. She is the Chair Professor of information science with the Wuhan University of Technology. She has authored more than 100 academic papers and books. Her research interests include signal processing, embedded systems, robots, and electronics. She was a recipient of two national awards and three provincial and ministerial awards.

YANG LIU is a graduate student with the School of Information Engineering, Wuhan University of Technology, China.

CHANG ZHU is a graduate student with the School of Information Engineering, Wuhan University of Technology, China.

XINGXING GUO is a graduate student with the School of Information Engineering, Wuhan University of Technology, China.

WEI MENG (Member, IEEE) received the joint Ph.D. degree in information and mechatronics engineering from the Wuhan University of Technology, Wuhan, China, and The University of Auckland, Auckland, New Zealand, in 2016. He was a Research Fellow in robotics with the School of Electronic and Electrical Engineering, University of Leeds, Leeds, U.K., from 2018 to 2020. He is currently an Associate Professor with the School of Information Engineering, Wuhan University of Technology. He has authored four monographs and over 60 peer-reviewed papers, and holds ten patents in rehabilitation robotics and human–robot interaction control.

QINGSONG AI (Member, IEEE) received the Ph.D. degree in information engineering from the Wuhan University of Technology, China, in 2008. He was a Visiting Researcher with The University of Auckland, New Zealand, from 2006 to 2007, and with the University of Leeds, U.K., from 2017 to 2018. He is currently a Professor of information engineering with the Wuhan University of Technology. He is also the Project Leader of 12 national, ministerial, or provincial projects. He has authored more than 70 international journals and conference papers.

JIWEI HU received the Ph.D. degree in electronic information engineering from The Hong Kong Polytechnic University, Hong Kong, in 2013. He is currently an Associate Professor with the School of Information Engineering, Wuhan University of Technology, China. He is the Project Leader or major partner of ten national, ministerial, or provincial projects. In the recent five years, he has authored over 20 academic papers. His research interests include pattern recognition, machine learning, and robot control.